Int. J. Electrochem. Sci., 7 **(2012)** 8299 - 8308

International Journal of
ELECTROCHEMICAL
SCIENCE
www.electrochemsci.org

Study on Surface Corrosion Behavior of Non-Charge-Discharge $LiMn_2O_4$ in $LiPF_6$-based Electrolyte

Ningning Wu[1, 2,*], *Bo Feng*[2], *Daojun Yang*[2], *Jianhong Liu*[2], *Wenhuai Tian*[1]

[1] Institute of Material Science and Engineering, University of science and technology, Beijing
[2] CITIC Guoan Mengguli Power Science and Technology Co., LTD, Beijing
[*]E-mail: wunn2010@163.com

Received: 16 July 2012 / *Accepted:* 16 August 2012 / *Published:* 1 September 2012

The surface corrosion behavior of non-charge-discharge $LiMn_2O_4$ spinel in $LiPF_6$-based electrolyte at elevated temperature is investigated. The change of non-charge-discharge $LiMn_2O_4$ spinel after soaking into 1.0 mol L^{-1} $LiPF_6$-based electrolyte at 55 ℃ for 10-30 days were studied with XRD, SEM, EDS, ICP and AC impedance. Compared with the pristine $LiMn_2O_4$, the chemical corroding reaction occurred in the soaking process, a fresh solid film formed on the non-charge-discharge $LiMn_2O_4$ surface, the lattice parameter of the corroded material decreased and the amount of dissolved Mn increased in electrolyte, which resulted in the impedance increased, the cycling performance and the discharge capacity of $LiMn_2O_4$ decreased. In this paper, we also conjectured the compounds of solid film, because of the chemical corroding reaction, the solid film is mainly composed of LiF and manganese fluoride.

Keywords: non-charge-discharge $LiMn_2O_4$; corrosion; solid film

1. INTRODUCTION

The spinel $LiMn_2O_4$ has been regarded to one of the most promising candidates of lithium ion battery (LIB) cathodes in the application of the electric vehicles (EVs) due to its Mn abundance, low toxicity, and good safety [1]. However, the cells used spinel $LiMn_2O_4$ as a cathode material have been known to cause severe capacity fading on charge–discharge cycling or storage, especially at high temperature. As we known, the lithium-ion battery is complex system, and the process of their fading is complicated. The capacity fading doesn't originate from one single cause, but from a number of various processes. For $LiMn_2O_4$ battery, numerous electrochemical and chemical processes influence the storage and cycling performance, including dissolution of Mn ion from $LiMn_2O_4$, crystal structure change of the cathode material and anode material, quality of surface film on the cathode and anode,

consumption of the electrolyte, degradation or changes of electrode components like conducting agents, binder, corrosion of current collector[2]. Indeed, these processes take place at same time and cannot be analyzed separately from each other. Recently, many research groups studied the mechanism of capacity fade in the $LiMn_2O_4$ battery [3-5], and proposed many available strategies for performance improvement of cycle and calendar life during an elevated temperature operation, which results in the increased lifetime of $LiMn_2O_4$ battery [6-8]. But the researchers are often ignore the effect of cathode surface film on the battery capacity fade, a considerable increasing of interfacial impedance was attributed to the cathode of lithium-ion battery [9][10]. Especially for $LiMn_2O_4$ battery, manganese dissolution would adversely affect the battery life, so the cathode interface film is very important. Now, few reports studied the surface corrosion behavior of non-charge-discharge $LiMn_2O_4$ in $LiPF_6$-based electrolyte at elevated temperature.

In this study, we focused on the chemical corrosion behavior of non-charge-discharge $LiMn_2O_4$ spinel in $LiPF_6$-based electrolyte at 55℃ and evaluated the effect of the electrochemical performance. Scanning electron microscope (SEM), X-ray diffraction (XRD), inductively coupled plasma atomic emission spectrometry (ICP-AES), Energy-dispersive X-ray spectroscopy (EDS) and AC impedance were used to analyze the surface morphology, structure, composition and impedance of the non-charge-discharge $LiMn_2O_4$ during before and after soaked. A possible compound of solid film on the soaked $LiMn_2O_4$ at 55 ^{0}C was conjectured.

2. EXPERIMENTAL

2.1. Experimental scheme

The $LiMn_2O_4$ spinel powder and $LiPF_6$-based electrolyte（1.0 mol L^{-1} $LiPF_6$ dissolves in a mixture of ethylene carbonate (EC), ethyl methyl carbonate (EMC) and dimethyl carbonate (DMC) (1:1:1, v/v)） are supplied separately by CITIC GUOAN Mengguli (MGL) and Kunlun Chem. The non-charge-discharge $LiMn_2O_4$ spinel powder is dried at 120 ℃ under vacuum over 24 h and then cooled off. The 50 g powder and 100 g $LiPF_6$-based electrolyte are sealed under vacuum in an aluminum plastic composite bag. Then the bag with $LiMn_2O_4$ spinel powder and electrolyte were placed into an oven maintained at a constant temperature of 55 ℃ for 10, 20, 30 days at 55 ℃. After stored several days ,the soaked powder is filtered (filter membrane pore size is 0.35μm) and washed with anhydrous DMC (99.98%) four times to remove residual electrolyte solvent and $LiPF_6$ salt followed by vacuum drying 48h at room temperature..

For electrochemical performance evaluation, half-cell studies are used to test EIS and cycling performance. The soaked powder is mixed with acetylene black and PVDF dissolving in NMP in the weight ratio of 90:5:5 to form slurry. After solvent evaporating, the electrode with aluminum current collectors is pressed and dried at 120 ℃ under vacuum over 24 h. CR2032-type coin cells are assembled in a glove box (M. Braun GmbH, Germany) with H_2O and O_2 content <1 ppm. Metallic lithium foil is used as counter electrode. The electrolyte is $LiPF_6$-based electrolyte and Celgard polyethylene is used as the separator.

2.2. Testing method

The structural changes of the soaked powder are analyzed by X-ray diffraction (XRD) using Cu Kα radiation (λ = 1.5406 Å) (D8 Advance, Bruker/German) with a scan speed of 2° min^{-1} between 10 and 90° at an applied potential of 40 kV and current of 40 mA. The step size is 0.02°, the divergence slit and anti-scatter slit is 0.6 and 8.0 mm separately. The surface morphology of the powders is observed by scanning electron microscopy (SEM, S-4800 microscope, Hitachi, Japan). Fourier transform infrared (FT-IR) spectroscopy of the samples is performed within wave number range 4000–400 cm^{-1} by using MAGNA-IR 560 from Nicolet of America. The composition of filtrate is analyzed using inductively coupled plasma mass spectrometry (ICP-MS, ELAN-DRC Ⅱ, PerkinElmer/America). AC impedance (EIS) is done by using the ZAHNER-IM6eX electrochemical workstation (Germany) at room temperature. The measurements are performed with 5 mV perturbation amplitude in the range from 200 kHz to 50 mHz in automatic sweep mode from high to low frequencies. Cycle life of the coin cells are tested using LAND CT2001A (5 V/10 mA).

3. RESULTS AND DISCUSSION

3.1 Analysis of the powders morphology and components

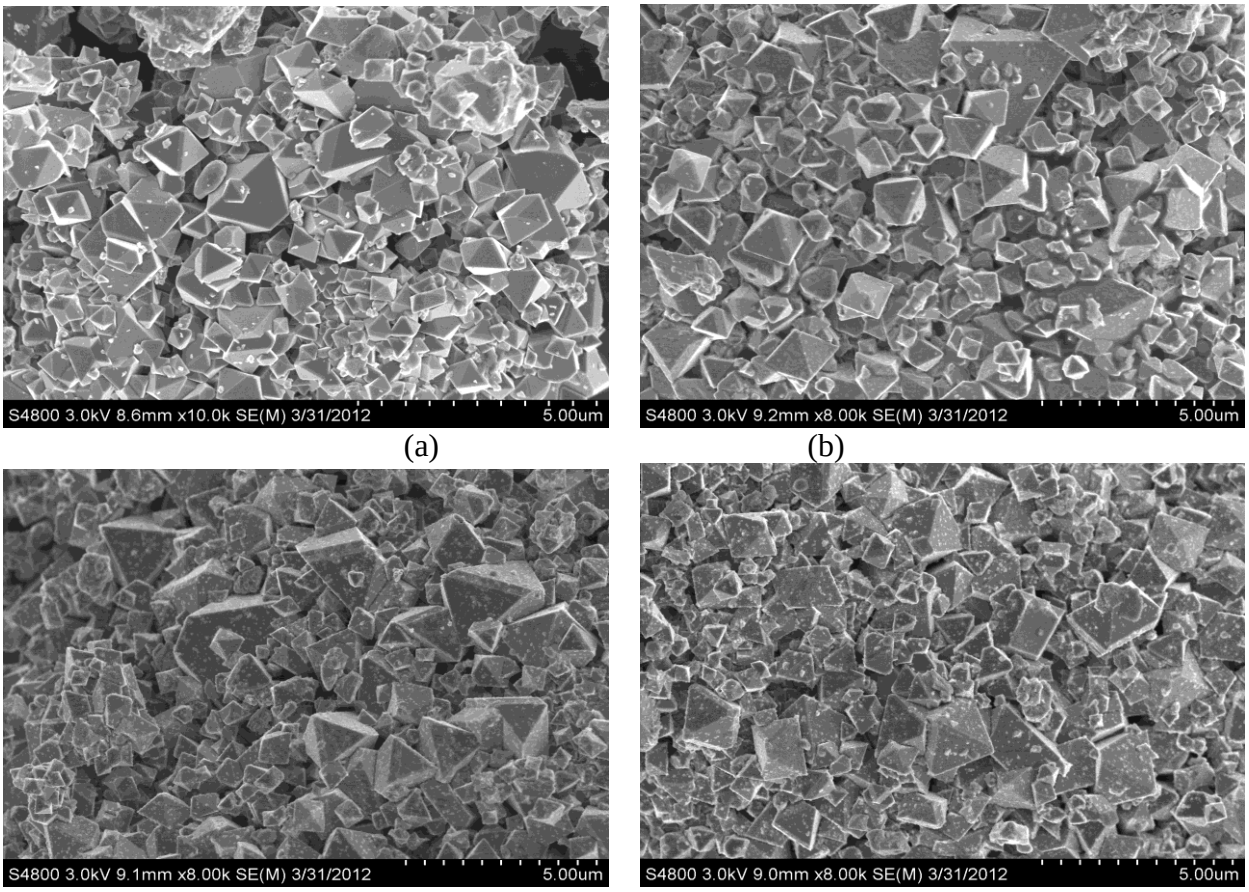

Figure 1. SEM of non-charge-discharge $LiMn_2O_4$: (a) pristine $LiMn_2O_4$, soaked at 55℃ for 10 (b), 20 (c) and 30 (d) days

The morphology of soaked powders was analyzed by SEM. Fig.1 (a) shows the pristine powder with a sharply and definitely shape of the spinel, and the surface is smooth. Fig.1 (b), (c), (d) shows the soaked materials at 55^0C for 10, 20, 30 days respectively, which exhibit a fresh solid layer on the particle surface and the film is getting thicker with the stored time extended.

Table 1. Concentration of Mn ions in the electrolytes of different soaking time at 55℃

	0 day	10 days	20 days	30 days
Mnμg **(L^{-1})**	63.6	899.5	1060.2	1814.5

The filtrated electrolytes after soaking spinel powders are analyzed using ICP-MS. The concentration of Mn ion increases when prolonging the soaking and storing time at 55^0C (Tab. 1), which attributed to the dissolving reaction of $LiMn_2O_4$ in electrolyte. Hence, the depositing reaction of Mn ions is simultaneous with the dissolving reaction. The dissolved Mn ions will worsen the cycling performance and storage behavior of batteries using the $LiMn_2O_4$ spinel as cathode.

Moreover, FT-IR spectra of pristine $LiMn_2O_4$ and soaked $LiMn_2O_4$ are tested (shown in Fig.2) in order to analyze components of the solid layer on the soaked $LiMn_2O_4$ powders. For bare $LiMn_2O_4$, the vibrations of the Mn-O and Li-O bands are located at about 615 cm^{-1}, 512 cm^{-1} and 1100 cm^{-1}, respectively [11-13]. The corroding reaction occurs and the solid products deposit on the surface of powders when $LiMn_2O_4$ is soaked in $LiPF_6$-based electrolyte at 55^0C. The absorption peaks of Mn(Ⅲ)-O and Li-O of soaked $LiMn_2O_4$ have a blue shift compared with the pristine spinel sample (Tab. 2), due to the forming of a solid layer on the surface of $LiMn_2O_4$ particles. The absorption peaks of Mn-O and Li-O of soaked $LiMn_2O_4$ are about the same value. Hence, it is reasonable to conclude that the chemical corroding reaction occurs mainly in the early days of the soaking process. The absorption peaks at about 1640 cm^{-1} and 3444 cm^{-1} are assigned to C=O and O-H vibrations. Some Li and Mn organic compounds with C=O and O-H groups deposit on $LiMn_2O_4$ powders soaking into electrolyte for 20 and 30 days at 55 ^{0}C.

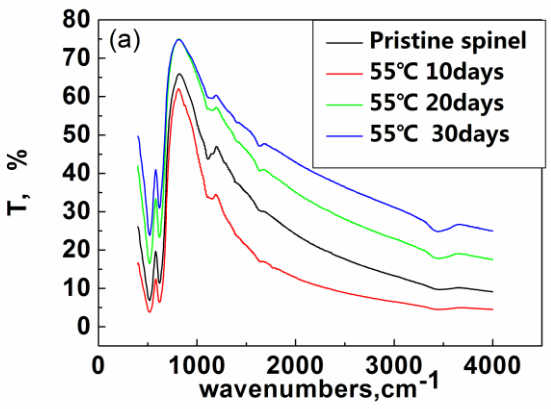

Figure 2. FT-IR spectra of pristine spinel and soaked powders

Tab. 2. Location of the FT-IR absorption peaks

	Mn(Ⅲ)-O	Mn(Ⅳ)-O	Li-O	C=O	O-H
Pristine spinel	517.80	619.05	1108.89	/	/
55℃,10 days	518.61	619.05	1152.28	/	/
55℃,20 days	518.77	619.05	1153.24	1638.26	3444.30
55℃,30 days	518.77	619.05	1153.24	1641.15	3442.37

3.2 Analysis of the solid layer on the soaked $LiMn_2O_4$ powders

The 10 g pristine $LiMn_2O_4$ powder and 10 g the soaked powder in $LiPF_6$-based electrolyte at 55 ^{0}C for 30 days are washed separately with 100 ml deionized water under ultrasonic waves for 2 h. Fig.3 shows the SEM of the soaked $LiMn_2O_4$ powder after being washed: (a) pristine $LiMn_2O_4$, (b) soaked at 55℃ at 30days. Compared with the no washing particle (Fig.1 (a)), the pristine $LiMn_2O_4$ after being washed have small changes with a sharply and definitely shape of the spinel, the surface is smooth. As $LiMn_2O_4$ soaked at 55^{0}C for 30days, the solid layer on the particle surface seems to have been dissolved, and the surface becomes rough. The deionized water after washing the non-charge-discharge $LiMn_2O_4$ powder was analyzed using ICP-AES method. The concentrations of Li and Mn ions increase sharply in the deionized water. The date was shown in Tab. 3. It reveals that the solid layer is mainly composed of some Mn and Li compounds. Mn and Li ions can dissolve from the $LiMn_2O_4$ powders when it is chemically corroded in $LiPF_6$-based electrolyte at 55^{0}C, and deposit on the particles.

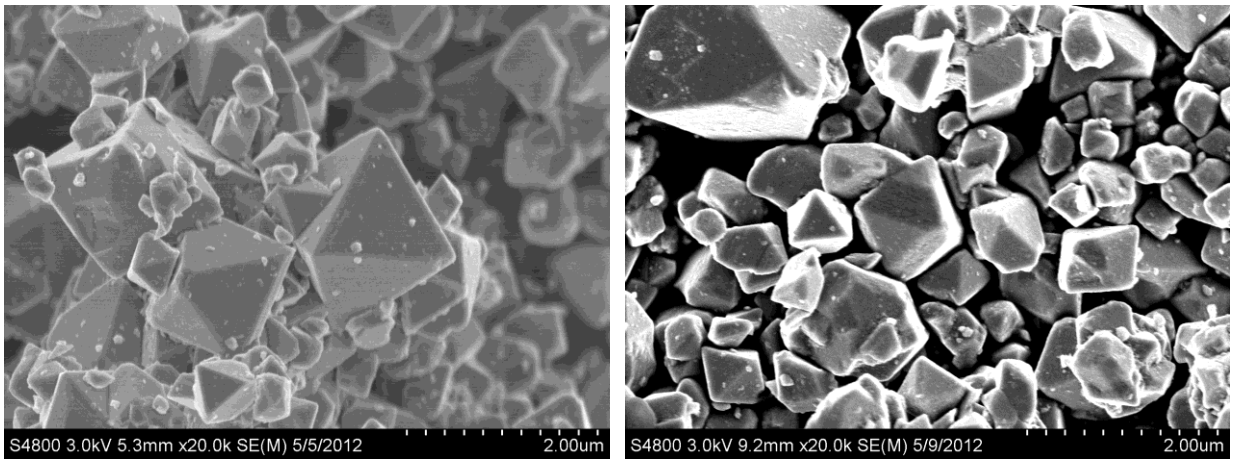

(a) (b)

Figure 3. SEM of $LiMn_2O_4$ spinel powder after being washed: (a) pristine $LiMn_2O_4$ (b) soaked at 55℃ for 30days

Table 3. Metal ion concentrations in the filtrates

Samples	Li (mg L^{-1})	Mn (mg L^{-1})
Pristine spinel	210.2	0.0778
Spine of being soaked 30 days	402.5	185.2

For elucidating the compounds of solid film, the EDS was used. Fig. 4 shows the EDS of $LiMn_2O_4$ spinel powder soaked at 55^0C for 30 days. The EDS results show that the material component of solid film on the particle surface is a compound composed of Mn, O and F.

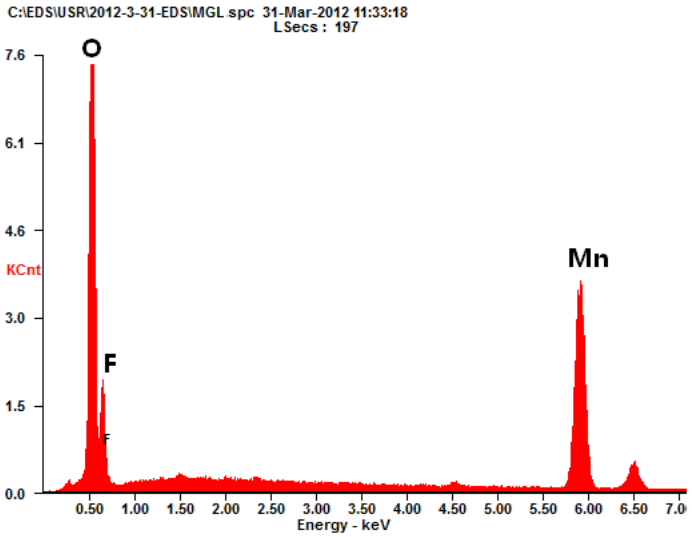

Figure 4. EDS of $LiMn_2O_4$ spinel powder soaked at 55℃ for 30 days

By ICP-AES analysis of the deionized water after washing the soaked $LiMn_2O_4$ powders, the solid layer is mainly composed of some Mn and Li compounds. Therefore, the compound of solid film was conjectured. Solid $LiPF_6$ is in equilibrium with solid LiF and PF_5 gas, the reaction temperature and the pressure of PF_5 gas determine the equilibrium position. Removal of PF_5 gas consumes $LiPF_6$ and produces LiF. For a $LiPF_6$ solution, the analogous equilibrium exists as shown in reactions (1). Because LiF is insoluble, only the concentration of $LiPF_6$ and PF_5 determine the equilibrium position. The traces water which comes mainly from the electrolyte and the powder surface reacts with PF_5 and yield HF as reactions shown in reactions (2) .So in electrolyte solutions, the equilibrium can move toward products LiF as PF_5 is consumed. The insoluble LiF deposits on the surface of $LiMn_2O_4$ powder. Traces of HF which comes from the $LiPF_6$ salt synthesis processare and reaction product react with spinel $LiMn_2O_4$ powder. The chemical corroding reaction occurred in the soaking process as shown in reactions (3). The reactions (1), (2) and (3) were accelerated at elevated temperature, which results in LiF and manganese fluoride depositing on the powders. The solid film is mainly composed of LiF and manganese fluoride[14].

$$LiPF_6 \rightarrow LiF \downarrow + PF_5 \uparrow \quad (1)$$

$$PF_5 + H_2O \rightarrow 2HF + POF_3 \quad (2)$$

$$2LiMn_2O_4 + 4HF \rightarrow 3\lambda\text{-}MnO_2 + MnF_2 + 2LiF + 2H_2O \quad (3)$$

3.3 XRD analysis of non-charge-discharge $LiMn_2O_4$

Fig. 5 shows the X-ray diffraction of spinel powders before and after being soaked. The data are analyzed with TOPAS software of Bruker. All the peaks in the XRD patterns of the $LiMn_2O_4$ were indexed as the spinel phase (JCPDS: 35-0782). These results indicate that the $LiMn_2O_4$ retains its spinel structure after being soaked. No additional peak in soaked cases is observed, yet the lattice constants (a) decrease compared with the pristine spinel powder. The change of lattice constant is caused by the Mn^{3+} ions dissolution from the spinel structure [15, 16]. The radius of Mn^{3+} is longer than that of Mn^{4+}. The lattice constants will decrease when Mn^{3+} dissolves from the $LiMn_2O_4$ [17]. This change of the $LiMn_2O_4$ structure makes Li-ion diffusion more difficult and charges transfer resistance increase. However, the lattice constants of soaked $LiMn_2O_4$ are about the same value, which does also prove that the chemical corroding reaction occurs mainly in the early days of the soaking process.

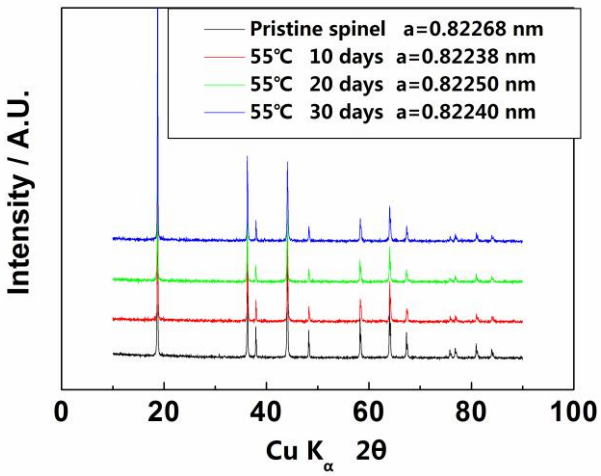

Figure 5. XRD patterns of pristine spinel and soaked powders

3.4 Analysis of the electrochemical impedance spectra

AC impedance measurement is carried out after the coin cells have been prepared. The data are analyzed with the ZSimpWin Software. The EIS plots (Fig.6) are fitted according to the equivalent circuit given in Fig.6 and the parameters are summarized in Tab.4. The impedance plot consists of a circular arc and an inclined line. The intercept at the Z' axis in high frequency corresponds to the ohm resistance (R_S), which represents the resistance of the electrolyte. The circular arc in the middle

frequency range indicates the resistance of solid layer (R_{SL}), the electron resistance (R_e) and charge transfer resistance (R_{ct}). The inclined line in the low frequency represents the Warburg impedance (Z_W) [18-20], which is associated with lithium ion diffusion in the cathode $LiMn_2O_4$ particles. In this work, the R_S values are almost the same throughout the experiments due to the same electrolyte and fabrication parameters, and they are around 5-8 Ω and much smaller than the R_{ct} values. The R_{SL} and R_{ct} values for the $LiMn_2O_4$ cathodes increase with the stored time extended. It can be attributed to the increasing of fluoride which results from dissolvable reaction of $LiMn_2O_4$ in electrolyte. The decrease of $LiMn_2O_4$ lattice constant maybe also make the charge transfer reaction at the electrode/electrolyte interface more difficult.

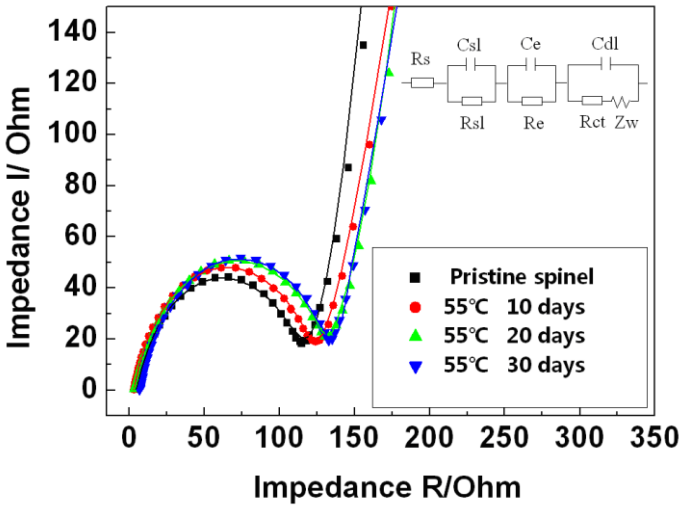

Figure 6. EIS of $LiMn_2O_4$/Li coin cells

Table 4. The impedance spectra parameters of $LiMn_2O_4$/Li coin cell

	Pristine spinel	55 ℃, 10 days	55 ℃, 20 days	55 ℃, 30 days
R_S (Ω)	6.027	3.929	4.831	7.626
R_{SL} (Ω)	14.5	86.6	97.9	117.9
R_e (Ω)	84.0	20.2	15.2	2.2
R_{ct} (Ω)	90.8	98.9	103.2	105.2

3.5 Cycling performance of $LiMn_2O_4$ (before and after being soaked) /Li coin cell

Fig.7 shows the discharge capacity and cycling performance of the $LiMn_2O_4$ (before and after being soaked) /Li. As the soaking and storing proceeded, the discharge capacity decreases and cycling performance worsen, which maybe result of the LiF and manganese fluoride depositing on the powders

and Mn^{3+} ions (origin of capacity) dissolving into electrolyte from the $LiMn_2O_4$ structure. These results agree with those from the analysis of XRD and EIS.

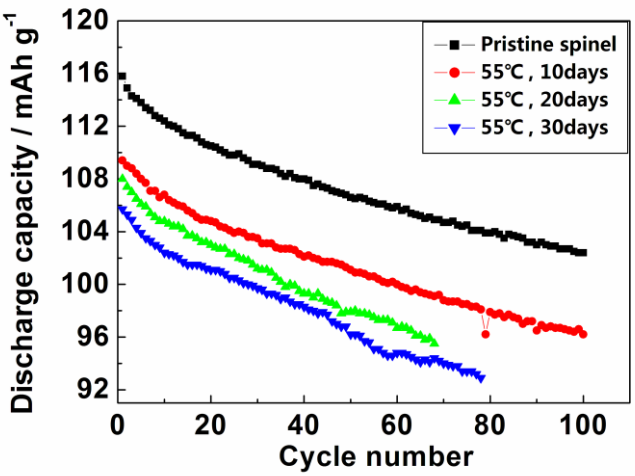

Figure 7. Cycling performance of $LiMn_2O_4$ (before and after being soaked) /Li coin cells (3.0-4.35 V, 55 ^{0}C)

4. CONCLUSIONS

In this work, the surface corrosion behavior of non-charge-discharge $LiMn_2O_4$ spinel in $LiPF_6$-based electrolyte at elevated was investigated. The discharge capacity and cycling performance of the $LiMn_2O_4$ after soaked decreased. The reason was studied with XRD, SEM, EDS, ICP and AC impedance. $LiPF_6$ salt is known to decompose slightly into LiF and PF_5 species which can further hydrolyze with traces of water to give more HF. The HF corrodes the $LiMn_2O_4$, and accelerated at elevated temperature. The chemical corroding reaction occurred in the soaking process, a fresh solid film formed on the $LiMn_2O_4$ surface, the lattice parameter of the corroded material decreased and the amount of Mn^{3+} ions dissolving into electrolyte, which result of the film resistance on the surface of $LiMn_2O_4$ and the charge transfer resistance increase. The compound of solid film is mainly composed of LiF and manganese fluoride.

ACKNOWLEDGMENTS
This work was supported by a grant from the National High Technology Research and Development Program of China (No. 2011AA11A230).

References

1. J.M. Tarascon, D. Guyomard, *J. Electrochem. Soc*, 138 (1991) 2864
2. J. Vetter, P. Nov´ak , M.R. Wagner , C. Veitb, K.-C. M¨oller, J.O. Besenhard, M. Winter, M. Wohlfahrt-Mehrens , C. Vogler , *J. Power Sources*, 147 (2005) 269–281
3. K. Edstrom, T. Gustafsson, J.O. Thomas, *Electrochimica Acta*, 50 (2004) 397
4. M. Herstedt, D.P. Abraham, J.B. Kerr, K. Edstrom, *Electrochimica Acta*, 49 (2004) 5097

5. K.Y. Chung, W.S. Yoon, K.B. Kim, B.W. Cho, X.Q. Yang, *J. Applied Electrochemistry*, 41 (2011) 1295
6. P. Barloux, J. M. Tarascon, F. K. Shokoohi, *J. Solid State Chem*, 94 (1991) 185
7. D.H. Jang, Y.J. Shin, S.M. Oh, *J. Electrochem. Soc*, 143 (1996) 2204
8. D.J. Lee, K.S. Lee, S.T. Myung, H. Yashiro, Y.K. Sun, *J. Power Sources*, 196 (2011) 1353
9. D.P.Abraham, R.D.Twesten, M.balasubramanian, I.Petrov, J.McBreen, K.Amine, *Electrichem. Commun*, 4 (2002) 620-625
10. C.H.Chen, J.Liu, K.Amine. *Electrichem.Commun*, 3(2001)44-47.
11. Z.S. Zheng, Z.L. Tang, Z.T. Zhang, *Electrochemistry*, 4 (2001) 433-438
12. A. Rougier, K.A. Striebel, S.J. Wen, T.J. Richardson, R.P. Reade, E.*J. Cairns*, *Appl. Surf. Sci*. 134 (2002) 107–115
13. C.M. Julien, M. Massot, *Materials Science and Engineering*, B97 (2003) 217-230
14. K. Xu, *Chem. Rev.*, 104(2004) 4303-4417
15. G.G. Amatucci, C.N. Schmutz, A. Blyr, C. Sigala, A.S. Gozdz, D. Larcher, J.M. Tarascon, *J. Power Sources* 69 (1997) 11
16. S. Komaba, N. Kumagai, T. Sasaki, Y. Miki, *Electrochemistry*, 69 (2001) 784
17. S. J. Hong, S.H. Chang, C.H. Yo, *Bull. Korean Chem. Soc.*, 20 (1999) 53
18. Q.C. Zhuang, T. Wei, G.Z. Wei, Q.F. Dong, S.G. Sun, *ACTA CHEMICA SINICA*, 67 (2009) 2184
19. F. Gao, Z.Y.Tang, *Electrochimica Acta*, 53 (2008) 5071
20. L. Wang, J.S. Zhao, X.M. He, J. Gao, J.J. Li, C.R. Wan, C.Y. Jiang, *J. Electrochem. Soc.*, 7 (2012) 345